JBC EDITORS' PICK

HIV-cell membrane fusion intermediates are restricted by Serincs as revealed by cryo-electron and TIRF microscopy

Received for publication, May 19, 2020, and in revised form, July 19, 2020 Published, Papers in Press, August 11, 2020, DOI 10.1074/jbc.RA120.014466

Amanda E. Ward[1], Volker Kiessling[1], Owen Pornillos[1], Judith M. White[2], Barbie K. Ganser-Pornillos[1,*], and Lukas K. Tamm[1,2,*]

From the Departments of [1]Molecular Physiology and Biological Physics and [2]Cell Biology, University of Virginia School of Medicine, Charlottesville, Virginia, USA

Edited by Craig E. Cameron

To enter a cell and establish infection, HIV must first fuse its lipid envelope with the host cell plasma membrane. Whereas the process of HIV membrane fusion can be tracked by fluorescence microscopy, the 3D configuration of proteins and lipids at intermediate steps can only be resolved with cryo-electron tomography (cryoET). However, cryoET of whole cells is technically difficult. To overcome this problem, we have adapted giant plasma membrane vesicles (or blebs) from native cell membranes expressing appropriate receptors as targets for fusion with HIV envelope glycoprotein-expressing pseudovirus particles with and without Serinc host restriction factors. The fusion behavior of these particles was probed by TIRF microscopy on bleb-derived supported membranes. Timed snapshots of fusion of the same particles with blebs were examined by cryo-ET. The combination of these methods allowed us to characterize the structures of various intermediates on the fusion pathway and showed that when Serinc3 or Serinc5 (but not Serinc2) were present, later fusion products were more prevalent, suggesting that Serinc3/5 act at multiple steps to prevent progression to full fusion. In addition, the antifungal amphotericin B reversed Serinc restriction, presumably by intercalation into the fusing membranes. Our results provide a highly detailed view of Serinc restriction of HIV-cell membrane fusion and thus extend current structural and functional information on Serinc as a lipid-binding protein.

To establish an infection, HIV must enter the cell by fusing its lipid membrane with a host cell membrane (1). HIV membrane fusion is mediated by conformational rearrangements in the viral envelope protein, Env, that are induced by binding to receptor, CD4, and co-receptor, CCR5 or CXCR4 (2). The process of HIV membrane fusion is thought to proceed through defined intermediate steps: receptor binding, hemifusion, and fusion pore opening and widening, similar to other enveloped viruses, such as influenza (3). The earliest step, receptor binding, has been visualized with nanometer resolution by electron tomography of plastic sectioned cells (4), but subsequent steps have not been directly observed. Fusion of influenza virus with its much simpler pH-sensitive fusion trigger has previously been studied by observing the merging of viral membrane envelopes with artificial liposomes using cryo-electron tomography (cryoET) (5–7), but HIV's requirement for two cell surface membrane proteins to trigger fusion has made *in vitro* reconstitution difficult. To examine fusion of HIV at the plasma membrane with cryoET, we have adapted giant plasma membrane vesicles (GPMVs or blebs) as model target membranes. Blebs are detached plasma membrane–derived vesicles that are much smaller than a cell and can easily be frozen in thin, vitreous ice required for cryoET. Blebs produced from cells expressing CD4 and CCR5 incorporate these full-length proteins along with their native lipid environment and post-translational modifications (8, 9). We reported earlier that the final fusion product of murine leukemia virus pseudoviruses bearing HIV Env and plasma membrane blebs can be visualized in projection by cryo-electron microscopy (9), and now show here that this system is ideally suited to image timed snapshots of 3D volumes, thus revealing multiple stages of the HIV fusion process by cryoET. In this study, we used a combination of cryoET and total internal reflection fluorescence (TIRF) microscopy with membrane blebs from HIV target cells to reveal various steps of fusion between two biological membranes, namely the HIV envelope and plasma membranes of susceptible cells. Tomograms of pseudovirus particles vitrified after different incubation times with $CD4^+/CCR5^+$ cell membrane blebs reveal a timeline of HIV fusion.

Serinc3 and Serinc5 are recently described viral restriction factors (10, 11) that are thought to block infection at cell entry, although the exact mechanism remains the subject of debate. Serincs comprise a family of plasma membrane proteins (12) that, in the absence of the HIV accessory protein, Nef, can incorporate into budding viral particles and decrease the infectivity of those progeny viral particles (13). Whereas isoforms Serinc3 and Serinc5 can block infection of subsequent cells, other isoforms, including Serinc2, do not. Previous work has suggested that Serincs may act at the very earliest steps of membrane fusion by changing the conformation or clustering of unliganded Env (14), as evidenced by increased binding of broadly neutralizing antibodies to Env on Serinc5-containing viral particles (15–17). Serincs are integral membrane proteins that have been reported to be involved in lipid synthesis (12). Indeed, the structure of Serinc5 features a lipid-binding groove involving 4 of its 10 transmembrane helices, and is stabilized by cholesterol, cardiolipin, and phospholipids (18). Despite these observations, when incorporated into viruses, Serincs do not appear to detectably alter the composition of the viral membrane (19). Some investigators have also suggested that Serinc

This article contains supporting information.

* For correspondence: Lukas K. Tamm, lkt2e@virginia.edu; Barbie K. Ganser-Pornillos, bkg7q@virginia.edu.

incorporation may change the distribution of Env in the viral membrane (20). Yet others have interpreted Serinc5's strong inhibition of infection to be indicative of an effect on fusion pore enlargement that would prevent delivery of the viral nucleocapsid into the cytosol (10, 11). This view was supported by the observation of impaired fusion pore formation using live cell imaging of HIV pseudovirus cell entry (17).

To elucidate at which step(s) Serincs might interfere with membrane fusion, we used a combination of TIRF microscopy and cryoET to monitor the evolution of fusion of viral particles with and without restricting and nonrestricting Serinc isoforms in their envelopes. With TIRF microscopy, we examine the fusion behavior of individual Serinc-containing and Serinc-lacking HIV pseudovirus particles to bleb-derived receptor– and co-receptor–containing supported planar plasma membranes (SPPMs) and find that Serinc3 and Serinc5, but not Serinc2, create bottlenecks to fusion at the hemifusion and at the pore expansion stage. Serinc3 and Serinc5, but not Serinc2, alter the progression of fusion and also reveal a subpopulation of new "cinched" structures not seen in the absence of Serincs. The combination of cryoET and TIRF microscopy on blebbed plasma membranes from receptor-expressing cells proved to be a powerful approach to reveal striking 3D images of membrane structures during restricted and unrestricted HIV fusion and thus provide structural as well as new functional insights into how Serincs restrict HIV entry into cells.

Results

Plasma membrane blebs as models for studying HIV membrane fusion

An ideal model target membrane for HIV fusion requires receptor, CD4, and co-receptor, CCR5 or CXCR4, in a lipid bilayer of size and geometry amenable to fluorescence and cryo-electron microscopies. Reconstitution of recombinant CD4 and CCR5 into proteoliposomes could produce such a model membrane but would be labor-intensive, technically difficult, and still generate lipid bilayers lacking many components of the target biological membrane. Production of GPMVs or blebs from HeLa cells is relatively simple (8), and such vesicles can be derived from cells that express CD4 and CCR5 (9). Blebs also have the advantage of featuring the native lipid composition of the plasma membrane and full-length proteins with appropriate post-translational modifications (Fig. 1*a*). We have previously established that blebs and SPPMs are good models for studying fusion of single murine leukemia virus particles pseudotyped with HIV Env in the absence of Serincs (9). To validate the fusion behaviors of HIV viral particles with and without Serincs for structural characterization by cryoET, we therefore turn first to their characterization by TIRF microscopy.

We prepared blebs from HeLa cells expressing CD4 and CCR5 as described under "Experimental procedures." Detached blebs were transformed from their spherical geometry into an SPPM by first depositing a lipid monolayer on a quartz slide via the Langmuir–Blodgett method, followed by spreading of the blebs on that monolayer (9) (see "Experimental procedures"). The resultant SPPM was then used as a target membrane with which to study single-particle fusion via TIRF microscopy (Fig. 1*b*). We modified our prior single-particle fusion assay by employing HIV pseudovirus particles that bear HIV Env and incorporate a freely diffusible mCherry content marker (21). When such particles were introduced into an SPPM from HeLa $CD4^+/CCR5^+$ cells, we observed a sudden appearance of punctate fluorescence, exemplified by the region of interest (ROI) shown in (Fig. 1*c*), indicating binding of the particle to the SPPM. The peak and mean intensities of the ROI shown in Fig. 1*c* are plotted over time in Fig. 1*d*. The fluorescence of the particle shown was stable over about 12 s, and then gradually declined to background fluorescence due to fusion and release of soluble mCherry into the cleft between the supported membrane and the quartz slide. Many such intensity traces were aligned to the onset of fusion, characterized by a peak due to initial content movement within the evanescent excitation field, and averaged (Fig. 1*e*). This average intensity was fit to a release model as described in Fig. S1, where mCherry is released into the aqueous cleft and allowed to diffuse laterally. Given the similarity of intensity traces of slow decay events to other previously published descriptions of single-particle viral fusion (22) and vesicle fusion (23) to supported membranes, we interpreted events such as those shown in Fig. 1 (*c–e*) to represent stable binding followed by membrane fusion and release of viral contents. Of the particles that bind to SPPMs, a higher fraction undergo fusion to CD4- and CCR5-containing membranes than to receptor-lacking membranes prepared in the same manner, which indicates this process is HIV receptor–dependent (Fig. 1*f*).

Observation of HIV membrane fusion by cryoET

Previous work has observed HIV particles bound to a T cell with multiple densities in between (4), but no work to date has directly observed subsequent steps of HIV membrane fusion and cell entry by cryoET. To obtain detailed snapshots of HIV pseudovirus particles in the act of membrane fusion, we employed GPMVs/blebs as target membranes for studying HIV fusion by cryoET. To increase the likelihood of observing short-lived fusion intermediates between CD4- and CCR5-containing blebs and HIV pseudoviruses, we synchronized fusion by prebinding pseudoviruses to blebs at 4 °C, raising the temperature to 37 °C for defined, brief times, and then immediately freezing the samples for cryoET. As fusion of multiple pseudovirus particles and blebs proceeds, one would expect the resulting membraned structure to be larger than the starting components, which is confirmed by the data shown in Fig. 2*a* (*red bars*). The average diameter of membraned particles increased as the mixture of pseudovirus and bleb was warmed for a longer time before freezing. This increase was blocked by the addition of the fusion-inhibiting peptide T20, which binds to the N-terminal heptad repeat region of HIV gp41, the transmembrane and fusion-promoting subunit of Env, and prevents the six-helix bundle formation that is required for fusion (24). Consistent with its described mechanism of action, T20-treated samples only showed receptor-mediated binding events (Fig. 2, *a* (*blue bars*) and *b*). Samples without T20 that were warmed for 10 s before freezing showed multiple structures that we interpret as receptor-mediated binding, hemifusion, and early fusion

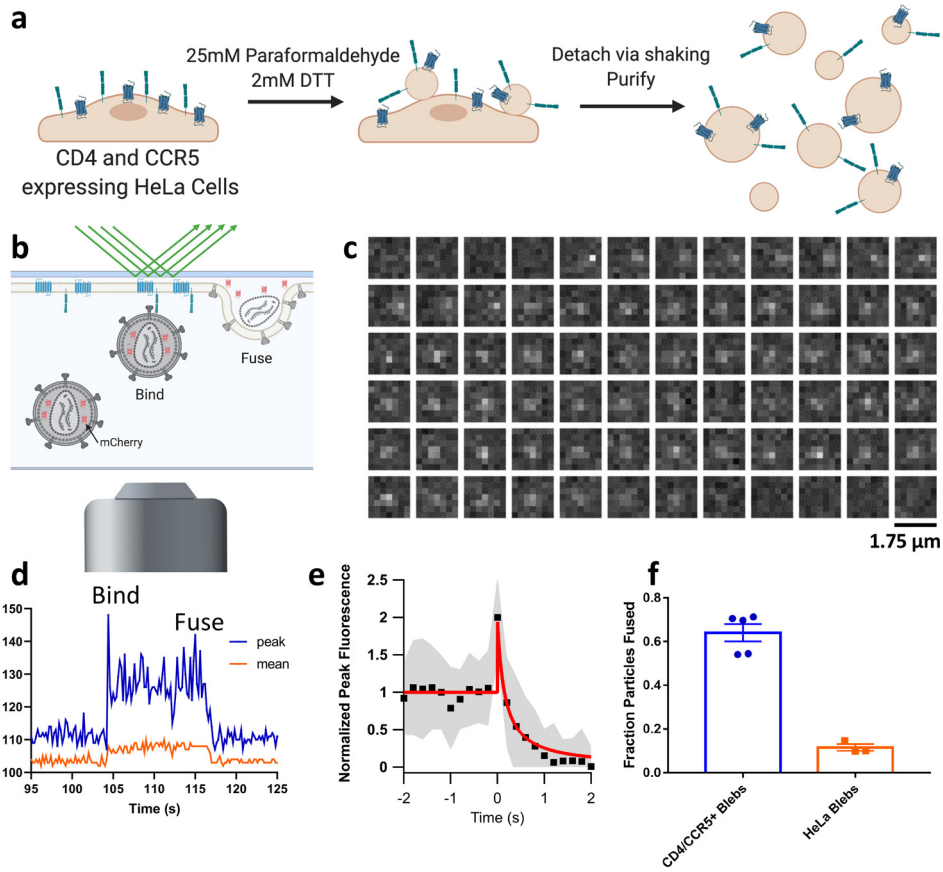

Figure 1. Membrane blebs as a model for studying viral fusion. *a*, *cartoon* depicting the protocol for making CD4- and CCR5-containing blebs from HeLa cells. Detached blebs are mixed with HIV pseudoviruses and frozen for cryoET or used to form a SPPM as shown in *b*. *b*, *cartoon* showing discrete steps of HIV fusion to a bleb-derived SPPM in a TIRF-based single-particle fusion assay. All pseudoviruses are grown with a genetically encoded soluble content marker, mCherry, that upon fusion diffuses out of the virus and into the cleft between the SPPM and the substrate (described in Ref. 21). *c*, example micrographs of an HIV pseudovirus particle with a diffusible mCherry content marker fusing with a CD4 and CCR5 containing SPPM. Each *box* represents the same region separated in time by 0.2 s. *d*, fluorescence intensity of the same particle is plotted over time, where *peak* is the intensity of the brightest pixel in the 7 × 7 region and *mean* is the average intensity of the same area. *e*, 30 intensity traces of fusing particles were aligned to the increase in intensity at the onset of fusion, averaged (*black squares* show the mean, *gray shaded area* shows S.D.), and fit to a release model as shown in Fig. S1 (*red line*). *f*, fraction of stably bound particles that undergo fusion to SPPMs made with blebs from CD4- and CCR5-overexpressing HeLa cells or HeLa cells that do not express either. Each *point* represents a separately prepared bilayer. *Error bars*, S.E.

products—whereas samples that were warmed for 30 s showed only some residual receptor-mediated binding events (Fig. 2*a*). Receptor binding at the later time point may represent defective pseudovirus particles that are incapable of fusion and thus remain attached to the bleb when other pseudoviruses have fused and are indistinguishable from blebs. The majority of tomograms of samples warmed to 37 °C for 30 s showed large-membraned particles that we deem late fusion products, which is consistent with measurement of those particle's diameters.

Examination of tomograms of T20-treated samples (Fig. 2*b* and Video S1) showed viral and target membranes in very close apposition but with a cleft between the densities separating the surfaces of both membranes. Additionally, densities extending from the viral membrane surface with a shape reminiscent of HIV Env (*orange arrow*) meet densities extending from the bleb membrane that intersect the Env-like density. There are no such densities in the area of closest approach of the two membranes. A similar scene was observed in tomograms of virus and bleb without T20 (Fig. 2*c* and Video S2), leading us to classify such interactions of virus and bleb as receptor-mediated binding, an early step of HIV fusion. In samples frozen 10 s after warming, we also observed events where there was no cleft between the membrane surfaces, but the line and curvature of the inner leaflet surfaces of the viral and bleb membranes were still clearly demarcated and not interacting (Fig. 2*d* and Video S3). Based on the similarity of these events to those observed in previous studies of influenza A fusion with liposomes by cryoET (7), we classify these events as hemifusion.

We observed a third class of events, where a single lipid bilayer surrounds contents of two different textures with a narrowing of the lipid bilayer around the transition between textures (Fig. 2*e*). The texture of the smaller lobe is reminiscent of the darker texture seen in viruses (Figs. 2, *b–d*), and densities extend from the membrane around the smaller lobe that could be HIV Env. Similar events were observed previously for influenza A membrane fusion with liposomes and classified as an early stage of fusion pore dilation (6), leading us to classify these events as an early fusion product, likely a step when the fusion pore is dilating and the viral matrix layer is dissociating. Similar events were also observed after herpes simplex virus-1 fusion to the plasma membrane of whole cells (25). In the samples warmed at 37 °C for 30 s before freezing, we observe some virus

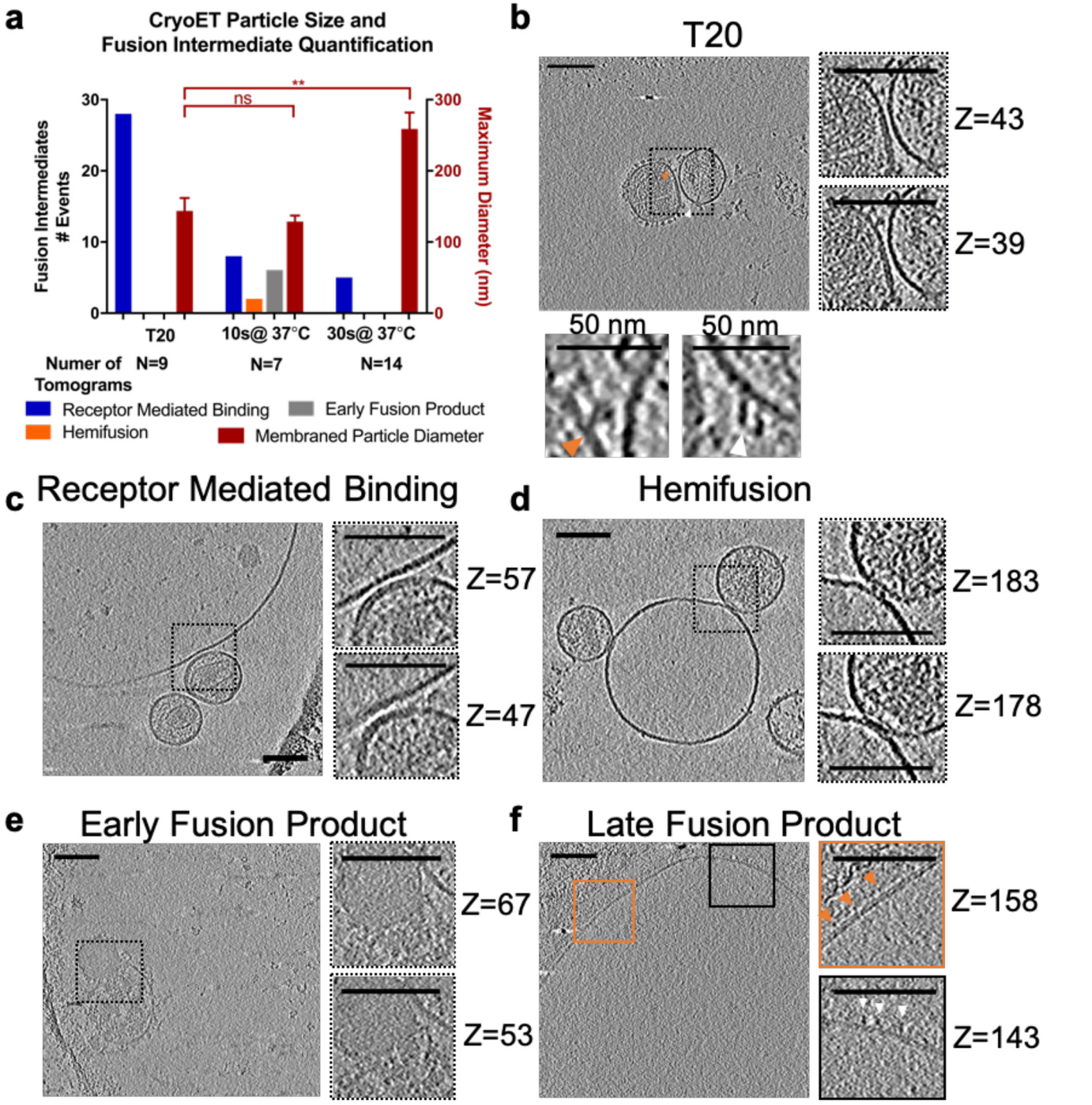

Figure 2. Observation of HIV membrane fusion intermediate structures by cryoET. *a*, membraned particle size and enumeration of fusion intermediates for each sample treatment. Spherical CD4- and CCR5-containing blebs were mixed with HIV pseudoviruses on ice and warmed to 37 °C for the indicated time before freezing on a grid for cryoET. The number of intermediate structures observed for each condition (*left y axis*) and the maximum diameter in the *z*-direction of membraned particles in a tomogram (*red bars* and *right y axis*) were plotted. Data are from one set of matched samples prepared and frozen at the same time and are taken from 109 similar tomograms. The number of tomograms for each treatment in this matched set is listed *below* the *x axis*. *Error bars*, S. E. Welch's *t* test is shown *above* data: **, $p < 0.01$; *ns*, not significant. Examples of each type of event are shown in *b–f*. *b–f*, *z*-slices through tomograms of HIV pseudovirus and blebs. Additional slices at *higher zoom* are shown on the *right* and *labeled* with their slice number in the *z*-direction. Tomograms are shown with cryoCARE denoising to enhance contrast for display. *Scale bars*, 100 nm unless otherwise indicated. Videos showing the complete tomograms and additional examples can be found in the supporting data. *b*, tomogram of V4 High Env HIV pseudovirus and bleb mixture treated with 135 ng/ml T20. To highlight densities suggested to represent Env (*orange arrow*) or densities that could potentially be CD4 (*white arrow*), higher-magnification views are shown *below* with a 50-nm *scale bar*. *c*, example tomogram showing characteristics used to classify receptor-mediated binding events. The mixture of HIV pseudovirus and blebs with 40 μM IP6 was warmed to 37 °C for 10 s before freezing. Defocus was −10 μm. *d*, example tomogram showing characteristics used to classify hemifusion events. The mixture of HIV pseudovirus and blebs with 40 μM IP6 was warmed to 37 °C for 10 s before freezing. Defocus was −10 μm. *e*, example tomogram showing characteristics used to classify early fusion product events. The mixture of HIV pseudovirus and bleb was warmed to 37 °C for 10 s before freezing. These types of events were relatively rare in the data set. Defocus was −6 μm. *f*, example tomogram of HIV pseudoviruses and blebs warmed to 37 °C for 30 s, which likely represents the product of multiple rounds of membrane fusion. Densities extend from the membrane that resemble HIV Env (*orange arrows*) and CD4 (*white arrows*). Defocus was −6 μm. Complete tomograms of *b*−*d* are presented in Videos S1–S3.

particles binding to blebs (Fig. 2*a*), but we mostly observe images such as seen in Fig. 2*f*, where there is a single, large-membraned particle. Closer examination of the densities protruding from the membrane show multiple mushroom-like densities that may be HIV Env (*orange arrows*) and others that resemble the Ig-fold of CD4 (*white arrows*). Given the increase in particle size at 30 s and the presence of densities in the unified membrane that could be contributed by both virus and bleb, we interpret similar structures to be the result of pseudovirus-bleb full fusion, likely the products of multiple rounds of virus and bleb fusion. Additional examples of HIV pseudovirus-bleb fusion intermediates are shown in Fig. S2.

Initial studies were performed with a HEK 293T–based packaging cell line that produces viral particles with 10-fold higher incorporation of HIV Env (26) (Fig. 2*b*), but we did not observe any increased fusion, as reported by mCherry release, with high Env pseudoviruses *versus* pseudoviruses produced from standard HEK 293T cells, so all subsequent studies were performed with SF162 HIV Env pseudoviruses produced from transiently transfected HEK 293T cells. In summary, using CD4- and CCR5-containing blebs as a target membrane to study HIV membrane fusion by cryoET, we have observed intermediates of HIV membrane fusion.

Effects of Serincs on HIV membrane fusion

We next applied both TIRF microscopy and cryoET to study fusion of Serinc-containing HIV Env pseudoviruses. There was a decrease in Serinc2- and Serinc3-containing HIV pseudovirus particles binding to CD4- and CCR5-containing SPPMs as compared with pseudoviruses that did not incorporate Serincs (Serinc-lacking) but no significant difference for Serinc5-containing pseudoviruses (Fig. 3*a*). However, of the particles that did bind, Serinc3- and Serinc5-containing pseudoviruses displayed impaired release of viral contents, whereas Serinc2 pseudoviruses had a similar fusion probability to Serinc-lacking viruses (Fig. 3*b*), as seen by Sood *et al.* (17) for Serinc5 and Serinc2, respectively. The magnitude of Serinc3 and Serinc5 restriction was titratable with transfection of increasing amounts of Serinc plasmid (Fig. S3*a*). For those viruses from Serinc-containing samples that did fuse, the kinetics of progression from binding to fusion pore opening were not appreciably different compared with those for Serinc-lacking pseudoviruses (Fig. 3*c*). Kinetics of viral content release are similar to previously published measurement of influenza A fusion to supported bilayers (22). The Serinc3 and Serinc5 particles that do fuse are a smaller subpopulation that could have lower Serinc incorporation. Infection of TZM-bl cells by the same preparations of HIV pseudovirus particles (Fig. 3*d*) recapitulated the SPPM fusion results (Fig. 3*b*), where Serinc3 and Serinc5 restricted HIV infection but Serinc2 did not, which is consistent with previously published infection results (10, 11, 15–17, 19, 27–30). Similarly, the size of membraned particles visualized by cryoET at 30 s after mixing of pseudovirus and blebs was notably smaller in tomograms of Serinc3- and Serinc5-containing pseudoviruses and blebs (Fig. 3*e*). Even at the later, 30-s time point when most Serinc-lacking viruses had progressed to late fusion products (Fig. 2*a*), we visualized many hemifusion and early fusion product events in tomograms with Serinc3 and Serinc5 pseudoviruses (Fig. 3*f*).

Most tomograms of Serinc2 pseudoviruses looked very similar to the late fusion products seen with Serinc-lacking pseudoviruses at the same 30-s time point (Fig. 3*g*); in 15 tomograms of Serinc2 samples, we observed only one early fusion product (Fig. 3*h*). Strikingly, some of the early fusion products observed in Serinc3 (Fig. 3, *i* and *j*) and Serinc5 (Fig. 3, *k* and *l*) tomograms show a cinching of membraned particles, and in the tomograms where viral capsids can be visualized, the capsid does not pass the narrowed section (Fig. S4). Together, the higher-resolution snapshots of Serinc-disrupted fusion obtained with cryoET and the information on the dynamic process of HIV pseudovirus fusion to SPPMs from TIRF microscopy show that Serinc3 and Serinc5 incorporation increases the likelihood of observing hemifusion and abnormal early fusion products and inhibits the opening of fusion pores large enough for passage of soluble mCherry.

Perturbations of membranes rescues HIV fusion from Serinc restriction

To better understand the step at which Serinc3 and Serinc5 restrict HIV fusion, we incorporated a fluorescent lipid, Atto488-dimyristoylphosphatidylethanolamine (DMPE), into the membrane of HIV pseudoviruses (Fig. 4*a*). Because membrane dyes have been reported to alter the efficiency and kinetics of viral fusion (31), we selected a phospholipid conjugated to a non-membrane-interacting fluorophore (32) that should have less of an effect on fusion, and indeed, we observed the same fusion efficiency for Serinc-lacking pseudoviruses whether or not they were labeled with Atto488-DMPE (Fig. S5). Fluorophore-conjugated phospholipids do not readily flip across a lipid bilayer (33), so the dye is largely confined to the outer leaflet of the viral membrane (Fig. S6). Upon lipid mixing of the viral and target membranes, as occurs during hemifusion, the punctate fluorescence of the membrane dye diffuses into the bilayer (Fig. S7). When dual mCherry- and lipid-labeled HIV pseudoviruses were allowed to fuse with an SPPM, no difference was seen in fusion probability between Serinc-lacking and Serinc-containing viruses, as reported by the membrane dye (Fig. 4*b*, *green bars*). However, incorporation of Atto488-DMPE increased the full fusion (content release) probability of Serinc3- and Serinc5-containing viruses as reported by the mCherry content marker (Fig. 4*b* (*red bars*) compared with Fig. 3*b*). This is in contrast to the behavior of mCherry singly labeled particles, where a clear diminution of content release was seen for Serinc3- and Serinc5-containing particles *versus* Serinc-lacking particles (Fig. 3*b*). Labeling the virus with Atto488-DMPE increases the speed of fusion pore opening of all types of pseudoviruses (Fig. 4*c*), but there are no significant differences in the speed of lipid mixing (*i.e.* hemifusion) of Serinc-lacking and Serinc-containing pseudoviruses as reported by the membrane dye (Fig. 4*d*). Changes in fusion probability and speed with Atto488-DMPE–treated pseudovirus could be the result of changes in lipid order of the viral membrane.

The antifungal agent amphotericin B is known to partition into membrane interfaces and to induce local changes in lipid order (34), as may occur in Atto488-DMPE–treated viruses. We found that 1 μM amphotericin B increased HIV pseudovirus infection of TZM-bl cells for Serinc5-containing pseudovirus with a trend toward increase for Serinc3-containing particles. In contrast, amphotericin B had little effect on the infectivity of Serinc-lacking or Serinc2-containing particles

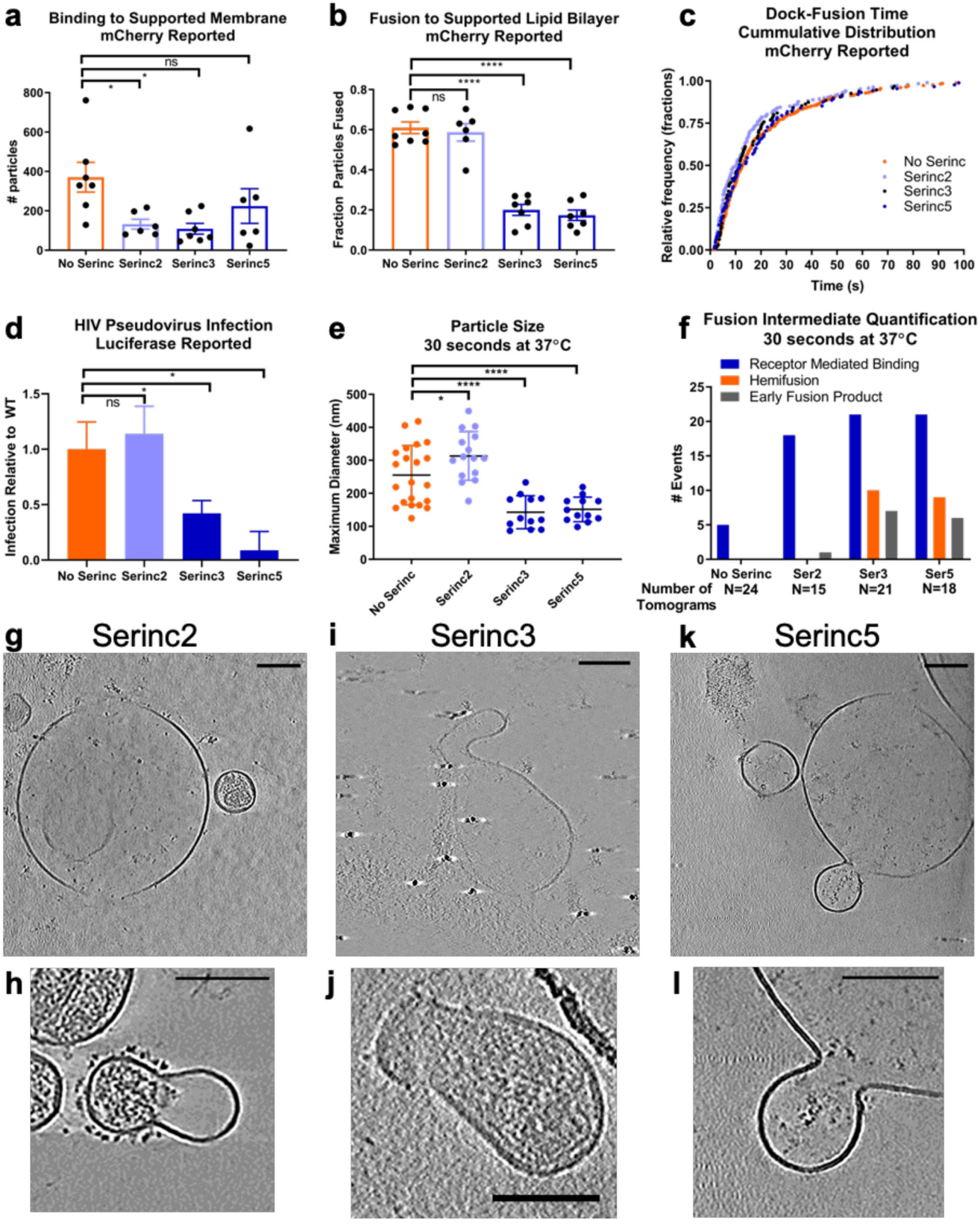

(Fig. 4*e*). In the single-particle SPPM fusion assay, 1 μM amphotericin B rescued fusion of Serinc3- and Serinc5-containing pseudoviruses but had no effect on Serinc-lacking or Serinc2 pseudoviruses (Fig. 4*f*). Therefore, it appears that perturbation of the viral membrane with lipophilic drugs, such as amphotericin B, or incorporation of exogenous lipids, such as Atto488-DMPE, can rescue Serinc3- and Serinc5-restricted HIV membrane fusion.

Discussion

In this study, we demonstrated that plasma membrane blebs are very useful biological target membranes to study HIV membrane fusion with the powerful combination of cryoET and TIRF microscopy. The two methods assess structural intermediates and correlate them with functional states, respectively. The necessity of two membrane protein receptors to trigger HIV fusion previously made *in vitro* reconstitution of HIV fusion challenging, but blebs from HIV target cells enable use of the full-length receptor (CD4) and co-receptor (CCR5) in multiple modalities. With such blebs, we have observed high-resolution snapshots of HIV membrane fusion intermediate structures and characterized the bottlenecks of HIV fusion caused by the HIV restriction factors, Serinc3 and Serinc5. This would likely not have been possible to achieve with whole cells because flash-frozen samples would have been too thick in most locations of a cell to result in high-resolution tomograms of a process that is rare and therefore hard to capture.

We observed an increase in the number and types of fusion intermediate structures visualized by cryoET in Serinc3- and Serinc5-containing samples (Fig. 3*f*) as well as a strong defect in content release from Serinc3- and Serinc5-containing particles by TIRF (Fig. 3*b*). This suggests that Serinc3/5 inhibit full fusion of HIV particles without targeting one particular step in the fusion process. It is already known that the energy required for each step during the fusion reaction increases along the fusion pathway (35, 36), so it is plausible that Serinc3/5 increase the energy barriers between the intermediate states. Consequently, most particles are unable to complete the final step (pore expansion) but instead populate intermediate states. Broad energetic changes could also explain the abnormal, "cinched," early fusion products observed by cryoET that appear unable to fully dilate a fusion pore (Fig. 3, *i*, *j*, *k* and *l*). These membrane structures are undetectable by TIRF microscopy because such wide fusion pores do not impede content (mCherry) release (Fig. S1) and could only be seen in the cryo-electron tomograms of HIV target cell membrane blebs.

Examination of the kinetics of fusion by TIRF microscopy shows no slowing of lipid mixing (Fig. 4*d*) or content release (Fig. 3*c*) of Serinc-containing viruses that do fuse under these conditions. One possible explanation is that the transition state energies of hemifusion and small fusion pore opening are unchanged by Serinc3/5. Together with the observation of hemifusion and cinched early fusion product events in tomograms of Serinc3- and Serinc5-containing virus at the later, 30-s time point, it may be that Serinc3/5-containing virus particles can complete the earlier intermediates of fusion but are slowed at later intermediate steps.

Interestingly, we discovered that treatment of HIV pseudoviruses with the membrane-partitioning antifungal amphotericin B has little effect on infection or fusion of Serinc-lacking pseudoviruses but increases infection and rescues fusion of Serinc3 and Serinc5 pseudoviruses, regardless of whether viral or target membranes are treated (Fig. 4, *e* and *f*). Because amphotericin B partitions into membranes and thereby alters the headgroup structure of the lipids at the membrane-water interface, this finding indicates that Serinc's inhibitory activity on membrane fusion likely involves its interaction with the membrane interface. This view is supported by similar results that were obtained by the lipid headgroup–altering fluorescent dye Atto488-DMPE. Whereas it was recently shown that Serinc5 itself selectively binds certain lipids (18), our results strongly suggest that Serinc-lipid interactions are important for HIV restriction. How exactly this membrane interactive activity of Serinc relates to the recently described lipid-binding grove on Serinc5 is not known and cannot be addressed with the methods employed in this study but would be interesting to follow up on in future experiments.

In summary, we revealed three-dimensional structures of various intermediates on the pathway of HIV virion to plasma membrane fusion at resolutions not previously seen. We also

Figure 3. Serinc incorporation enhances the probability of observing hemifusion and abnormal early fusion products. *a*, number of HIV pseudovirus particles that bound to a CD4- and CCR5-containing SPPM. An equal amount of pseudovirus as measured by HIV p24 was introduced to bilayers and observed by TIRF microscopy for 13.3 min. HIV pseudovirus particles used in this experiment were labeled only with an mCherry content marker. Each *point* represents a separately prepared SPPM. Three separate preparations of each type of pseudovirus were examined. *b*, fraction of bound HIV pseudovirus particles that underwent fusion, as reported by loss of mCherry content marker. Each *point* represents a separately prepared SPPM. Data were collected from five experiments from three separate preparations of each type of pseudovirus. *c*, single-particle kinetics of pseudovirus fusion. The time between docking and the beginning of fusion, as reported by loss of mCherry signal, was measured for individual viral fusion events; each *point* represents an event. Events from five experiments and three separate HIV pseudovirus preparations are shown for each type. In total, 336 Serinc-lacking events, 187 Serinc2 events, 95 Serinc3 events, and 88 Serinc5 events are shown. *d*, infection of TZM-bl reporter cells by an equal amount of each type of HIV pseudovirus as measured by HIV p24. Data shown are from three separate preparations of pseudovirus and three infection experiments. For each experiment, the luciferase signal was normalized to the Serinc-lacking signal from a parallel preparation of virus examined in the same experiment. *Error bars*, S.E. *e*, maximum diameter in the *z*-direction of membraned particles in a tomogram after mixing with CD4- and CCR5-containing blebs and warming to 37 °C for 30 s before freezing for cryoET. Each *point* represents a tomogram. *Error bars*, S.E. *f*, enumeration of fusion intermediate structures observed in tomograms of Serinc-lacking or Serinc-containing HIV pseudoviruses. The number of tomograms for each treatment is listed *below* the *x axis*. *g*–*l*, *z*-slices through tomograms of Serinc-containing HIV pseudovirus and blebs that were warmed to 37 °C for 30 s before freezing for cryoET. Tomograms are shown with cryoCARE denoising to enhance contrast for display except where noted. *Scale bars*, 100 nm. *g*, representative image of tomograms of Serinc2-containing HIV pseudoviruses; *h*, the only early fusion product event observed in all tomograms of Serinc2 pseudoviruses and blebs. Both tomograms were prepared with 40 μM IP6 and acquired at -10 μm defocus. *i* and *j*, representative images of early fusion products of Serinc3-containing pseudoviruses from different tomograms. *i* was acquired with -4 μm defocus, and *j* was prepared with 40 μm IP6, taken at -10 μm defocus, and is shown with nonanisotropic diffusion filtering. *k*, representative image of an early fusion product of Serinc5-containing pseudovirus and blebs. *l*, an enlargement of the *image in k*. The tomogram was taken at -5 μm defocus. Welch's two-tailed *t* test is shown *above* data: $p < 0.05$; **, $p < 0.01$; ****, $p < 0.0001$; *ns*, not significant. Complete tomograms of *g*, *i*, and *k* are presented in Videos S4–S6.

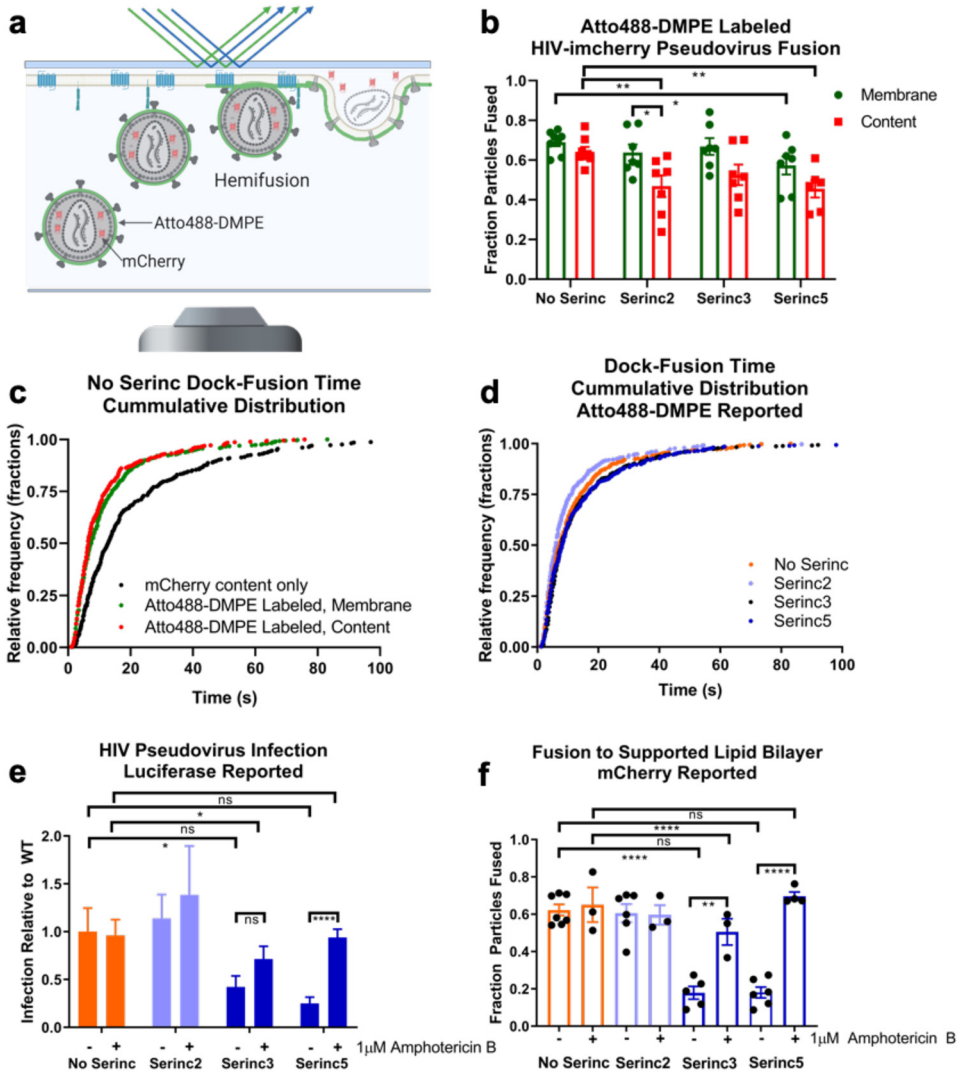

Figure 4. Perturbation of the viral membrane rescues HIV fusion and infection from Serinc restriction. *a*, *cartoon* depicting SPPM fusion experiment with double-labeled HIV pseudovirus. Because the vast majority of the Atto488-DMPE fluorescent membrane dye is in the outer leaflet of the viral membrane (supporting data), both hemifusion and full fusion are reported as decay of the Atto488 fluorescence. Only full fusion is reported as decay of mCherry fluorescence. *b*, fraction of bound HIV pseudovirus particles that underwent fusion, as reported by loss of mCherry content marker (*red*) or lipid mixing, as reported by loss of Atto488 fluorescence from membrane dye (*green*). Data are from four separate experiments with two technical replicates for each. *Error bars*, S.E. Unpaired two-tailed *t* test is shown *above* data. All comparisons not shown are not significant. *c*, comparison of single-particle kinetics of Atto488-DMPE–labeled *versus* non-membrane-labeled pseudovirus fusion. The time between docking and the beginning of fusion was measured for individual viral fusion events. Each *point* represents an event, and events are from four experiments. In total, 462 mCherry content only (unlabeled) events, 536 membrane-reported fusion events from Atto488-DMPE–labeled pseudovirus, and 330 content-reported fusion events from Atto488-DMPE–labeled pseudovirus are shown. *d*, single-particle kinetics of Atto488-DMPE–reported pseudovirus fusion. The time between docking and the beginning of lipid mixing was measured for individual viral fusion events; each *point* represents an event, and events are from four experiments. In total, 536 Serinc-lacking events, 373 Serinc2 events, 459 Serinc3 events, and 485 Serinc5 events are shown. *e*, infection of amphotericin B–treated TZM-bl cells by Serinc-containing or -lacking HIV pseudoviruses. Cells were pretreated with 1 μM amphotericin B for 30 min before spinfection with HIV pseudoviruses, also in medium with 1 μM amphotericin B. Data shown represent three separate preparations of pseudovirus and three infection experiments. Untreated data are replotted from Fig. 3*d* for comparison. *Error bars*, S.E. Paired two-way *t* test is shown *above* data. *f*, fraction of bound HIV pseudovirus particles that underwent fusion, as reported by loss of mCherry content marker. Each *point* represents a separately prepared SPPM. Untreated data are replotted from Fig. 3*b* for comparison. Amphotericin B–treated data were collected from three experiments from three separate preparations of each type of pseudovirus. Unpaired two-tailed *t* test is shown *above* data: *, $p < 0.05$; **, $p < 0.01$; ****, $p < 0.0001$; *ns*, not significant.

demonstrated that the viral envelope–embedded restriction factors Serinc3 and Serinc5 arrest fusion at more than one of these intermediate structures, suggesting an underlying mechanism with broad-reaching changes to the energetics of fusion. These results provide a new dimension to explain the mechanism of Serinc's viral restriction function. In the process, we also showed that plasma membrane blebs are useful for studying HIV membrane fusion in 3D by both cryoET and TIRF microscopy. The TIRF data on the dynamics of fusion and the static cryoET snapshots of multiple fusion intermediate structures complement each other. The methodology we developed could easily be used to study membrane fusion and cell entry of other viruses, other types of membrane fusion, and plasma membrane functions, such as endocytosis, clustering of receptor signaling molecules, and potentially, conformational changes of ion channels.

Experimental procedures

Cell lines, reagents, and plasmids

HEK 293T/17 cells (ATCC) were maintained in high-glucose Dulbecco's minimum essential medium (Gibco) supplemented with 10% fetal bovine serum (Atlanta Biologicals), 1% antibiotic-antimycotic (Gibco), 1 mM sodium pyruvate (Gibco), and 2 mM glutamine (Gibco). V4 high HIV Envelope cells were a gift from Michael Zwick (26) and were maintained in the same medium as the HEK 293T/17 cells supplemented with 1 μg/ml puromycin (Gibco). HeLa cells (ATCC), TZM-bl cells (AIDS Reagents Program), and CD4- and CCR5-overexpressing HeLa cells (gift of David M. Rekosh, University of Virginia) were maintained in Iscove's modified Dulbecco's medium (Gibco) supplemented with 10% fetal bovine serum and 1% antibiotic/antimycotic. The medium of the CD4- and CCR5-overexpressing HeLa cells was supplemented with 0.5 mg/ml G418 (Gibco) and 1 μg/ml puromycin. All cells were maintained at 37 °C with 5% CO_2 atmosphere.

pHIV-luciferase, pHIV-Rev, and pHIV-pack were gifts of Wen Yuan (University of Virginia). pHIV-Env-SF162 was provided by the AIDS Reagent Program. pHIV-imCherry (37) was a gift of Gregory Melikian (Emory University), pPBJ5-Serinc2-HA was a gift of Massimo Pizzato (University of Trento), and pPBJ5-Serinc3-HA and pPBJ5-Serinc5-HA were gifts of Heinrich Gottlinger (University of Massachusetts Medical School, Worcester, MA, USA).

HIV pseudovirus preparation

HIV pseudoviruses were produced by transfection of HEK 293T cells (ATCC) with Lipofectamine 2000 (Invitrogen) and the following amounts of plasmids per 10-cm dish: 13 μg of pHIV-luciferase, 5 μg of pHIV-pack, 4 μg of pHIV-Env-SF162 (38–40), 4 μg of pHIV-imCherry, 1 μg of pHIV-Rev and 4 μg of pBJ5-Serinc2-HA (11), pBJ5-Serinc3-HA (10), or pBJ5-Serinc5-HA (10) as indicated in the text. "High Envelope" HIV pseudoviruses were produced in the previously described V4 cell line (26) with the same amounts of plasmids excluding pHIV-Env-SF162. Culture medium was changed 4–6 h after transfection to phenol red–free Dulbecco's modified Eagle's medium supplemented with 10% FBS, 1% antibiotic-antimycotic, 1 mM sodium pyruvate, and 2 mM glutamine. Culture supernatants were harvested 2 days after transfection and cleared by centrifuging at 5000 × *g* before passing through a 0.22-μm filter. HIV pseudoviruses were pelleted through a 25% sucrose-HME (20 mM HEPES, 20 mM MES, 130 mM NaCl, 1 mM EDTA (pH 7.4)) cushion as described previously (41) and resuspended in buffer HME without sucrose. Pseudovirus preparations were further purified by density-dependent centrifugation on a discontinuous sucrose gradient composed of 65% sucrose-HME and 25% sucrose-HME spun at 151,000 × *g* for 18 h. Pseudovirus was collected from the 65%/25% sucrose interface, diluted in HME buffer without sucrose, and repelleted through a 25% sucrose cushion. After resuspension in HME buffer without sucrose, the pseudovirus preparation was aliquoted and stored at −80 °C. Additionally, the concentration of HIV p24 in each preparation was measured by ELISA (42, 43) and used to normalize the amount of pseudovirus added to downstream experiments. Each preparation of virus was checked for incorporation of Serincs by Western blotting against the HA tag (Fig. S8) with a rat anti-HA antibody (3F10, Roche Applied Science) normalized to p24 as detected by human anti-HIV immune globulin (AIDS Reagent Program) (44). For some preparations of virus, a small amount was surface-biotinylated with sulfo-NHS-LB-Biotin (Thermo Scientific) before Western blotting with detection by streptavidin-IR680 (LI-COR Biosciences).

Infection of TZM-bl cells (45–48) by HIV pseudoviruses was performed as described previously (49), and firefly luciferase activity was measured 2 days postinfection with the BriteLite reagent (PerkinElmer Life Sciences) in a plate reader (Flex Station M5, Molecular Devices). Pelleted HIV pseudovirus preparations were diluted in Opti-MEM (Gibco) to the same concentration of p24 to ensure equal loading of viral particles. For infection assays performed with amphotericin B (Bio Basic), cells were pretreated with 1 μM amphotericin B diluted in Opti-MEM or Opti-MEM alone for 30 min before HIV pseudoviruses, diluted in 1 μM amphotericin B in Opti-MEM or Opti-MEM alone, were added.

For some TIRF experiments, a fluorescent membrane label, Atto488-DMPE (Millipore–Sigma), was incorporated into the viral membrane. Atto488-DMPE was dried on the bottom of a glass test tube to remove chloroform/methanol solvent and resuspended in buffer HB (20 mM HEPES, 150 mM NaCl (pH 7.4)) to a concentration of 1.8 μg/ml. HIV pseudovirus was diluted to a concentration of 2 μg/ml, as measured by p24, in buffer HB and mixed in a 1:3.5 ratio with the dye suspension. The mixture was incubated at room temperature in the dark for 2 h on a rotary spinner. To remove free Atto488-DMPE, the HIV pseudovirus mixture was diluted up to 1.5 ml in buffer HB and pelleted by spinning at 21,000 × *g* for 1 h at 4 °C. The viral pellet was washed in an additional 1.5 ml of buffer HB and pelleted again. Atto488-DMPE–labeled HIV pseudoviruses were used within 24 h. For TIRF experiments with Atto488-DMPE–labeled virus, the chamber with the SPPM was washed with 3 ml of buffer HB and allowed to equilibrate before pseudovirus was introduced.

Plasma membrane bleb preparation

Blebs were produced from HeLa cells (ITCC) or HeLa cells overexpressing CD4 and CCR5 by previously published methods (8, 9). Briefly, when cells reached 90% confluence, they were washed twice with blebbing buffer (10 mM HEPES, 150 mM NaCl, 2 mM $CaCl_2$, pH 7.4), and blebbing was induced by replacing buffer on the cells with 5 ml of 25 mM formaldehyde (J. T. Baker) and 2 mM DTT diluted in blebbing buffer and incubating the cells at 37 °C, 5% CO_2 for 45 min. After 45 min, blebs were detached from cells by shaking on a radial shaker at room temperature for 1 h before the supernatant was collected and cleared of large cell debris by centrifuging at 100 × *g* for 10 min. Blebs were pelleted at 20,000 × *g* for 1 h and washed twice in blebbing buffer without DTT or formaldehyde. Blebs used for cryoET were washed and resuspended in blebbing buffer without calcium and filtered through an 800-nm filter. For select cryoET experiments, 40 μM inositol hexaphosphate (IP6) was added to wash and resuspension buffers.

TIRF-supported lipid bilayer fusion assay

Supported planar plasma membranes derived from blebs were prepared as described previously (9, 50, 51). Quartz slides were cleaned in piranha solution (95% H_2SO_4 and 30% H_2O_2 in a 3:1 ratio) and rinsed in 12 liters of deionized water. Next, a lipid monolayer composed of 4:1 brain phosphatidylcholine and cholesterol (Avanti Polar Lipids) with 3% 1,2-dimyristoyl-*sn*-glycero-3-phosphoethanolamine-PEG3400-triethoxysilane was deposited on the quartz slide by the Langmuir–Blodgett method. A chloroform solution of the lipid mixture was applied to a Nima 611 Langmuir–Blodgett trough, and after letting the solvent evaporate for 10 min, the lipid layer was compressed at a rate of 10 cm^2/min to a pressure of 32 millinewtons/m. A cleaned, rinsed, and dried quartz slide was rapidly dipped (68 mm/min) and slowly removed (5 mm/min) from the trough and then dried in a desiccator chamber overnight.

The slide was then assembled into a custom-built microscopy flow cell, and plasma membrane blebs diluted in blebbing buffer without DTT or formaldehyde were flowed in to form the outer leaflet of the supported planar plasma membrane. After 2 h at room temperature, the flow cell was washed with multiple volumes of blebbing buffer and then multiple volumes of HME buffer and transferred to a prism-based TIRF microscope. The sample was excited with a 561-nm diode laser (OBIS 561 nm LS, Coherent) at an angle of 72° from normal, and emission light was filtered through a dichroic mirror (DC565, Semrock) and a band-pass filter (BP605/50, Semrock). For double-labeled (membrane and content) experiments, the sample was excited with both a 488-nm (OBIS 488 nm LX, Coherent) laser and the 561-nm laser. Emission light from both labels was filtered by a dichroic mirror (DC-Di-493/574, Semrock) before the combined light was split into two bands by an optosplit (Optosplit II, Andor Technology) equipped with a dichroic mirror (DC562, Semrock) and two band-pass filters (BPS525/50 and BP607/70, Semrock). Video was recorded by an EMCCD (DV887ESC-BV, Andor Technology) in frame transfer mode with an exposure time of 0.2 s for 13.3 min as a dilution of HIV pseudovirus totaling 16 ng of p24 as measured by ELISA was flowed into the chamber. Laser intensity, shutter, and camera were controlled by a custom LabView program (National Instruments).

Intensities of single particles over time were extracted with a custom-built LabView program and classified as representing binding without fusion or binding with fusion based on the following criteria: a rapid increase in intensity followed by multiple frames of similar intensity without translation of the particle more than 4 pixels was classified as binding. If the intensity of the particle remained the same for the duration of the acquisition or slowly bleached over 10 s or more, this was considered binding without fusion. If the intensity of a bound particle decreased to background in one frame (0.2 s), this was considered an unbinding event. If the intensity of a bound particle decreased to background with a characteristic curve as shown in Fig. 1*e*, it was classified as binding with fusion.

CryoET of HIV pseudoviruses and membrane blebs

Temperature was used to synchronize HIV membrane fusion before freezing. HIV pseudovirus particles were mixed with 10-nm colloidal gold fiducials and CD4- and CCR5-containing membrane blebs in a thin-walled PCR tube on ice for 1 min. The PCR tube was then transferred to a heat block set at 37 °C for either 10 or 30 s. The HIV/bleb/gold mixture was rapidly transferred to a C-Flat 2/2-3C or Quantifoil 2/2 grid (Electron Microscopy Sciences), previously glow-discharged with amylamine (Sigma), blotted, and frozen in liquid ethane before storage in liquid nitrogen. To aid the visualization of viral capsids, 40 μM IP6 (52) was added to the membrane blebs before freezing for some samples as it is expected to leak out of blebs (53). The grids were imaged on a Titan Krios electron microscope operating at 300 kV equipped with a Falcon 3 detector and controlled by Tomography 4.0 software (Thermo Fisher Scientific). Bidirectional tilt series of regions of interest were acquired with 2° increments from −60 to +60°. Magnification was ×29,000, which yielded a pixel size of 0.288 nm.

Tilt series images were motion corrected with MotionCor2 (54) (5 × 5 patch for 10 iterations with a tolerance of 0.5), and tomograms were reconstructed in IMOD (55). High-tilt views that were obstructed were excluded. Gold fiducials were used for alignment. Aligned tilt stacks were binned by 4 and back-projected to create tomograms. To enhance contrast for display, tomograms were denoised by cryoCARE (56) with the following parameters: binned by 6; training volumes, 1200; validation volumes, 120; volume dimensions, 64 × 64 × 64; training epochs, 200; steps per epoch, 75.

Classification criteria for HIV fusion intermediate structures shown by cryoET

Receptor-mediated binding—One membraned vesicle must be ~100–150 nm in diameter and show a continuous, medium density texture inside the membrane; we classify this as a viral particle. The target membrane vesicle can be any size and must have a less regular and lower density texture inside. At least one instance where a dark, linear density extends between viral and target membranes is required. This distinguishes particles that may be close by chance from those that are interacting. We did not distinguish between loose binding or tight binding.

Hemifusion—Using the same definition of viral particle and target membrane above, hemifusion is defined such that there is at least one section through a tomogram (binned by 4) where the densities of the outer lipid leaflets of viral and target membranes are indistinguishable but the curvature of the inner leaflet is unchanged.

Early fusion product—There must be only one contiguous membrane, and it cannot be spherical but rather have some sort of narrowing. There must be either 1) demarcation of different textures within the volume surrounded by the membrane, 2) clear evidence of viral products like a capsid within the membrane, or 3) virus-like membrane proteins in a lobe of ~100 nm in diameter.

Late fusion product—There must be only one contiguous membrane, and it must be approximately spherical without

focal narrowing. It must be much larger than a virus (>200-nm diameter). It must have some evidence of viral proteins, whether that is characteristic Env-like densities in the membrane or virus-like textured density inside.

Acknowledgments—We thank Dr. Marie-Louise Hammarskjold and Dr. David Rekosh for the gift of CD4- and CCR5-overexpressing HeLa cells and Dr. Heinrich Gottlinger, Dr. Gregory Melikyan, and Dr. Massimo Pizzato for the gift of pBJ5-Serinc plasmids. The following reagents were obtained through the National Institutes of Health AIDS Reagent Program, Division of AIDS, NIAID, National Institutes of Health: TZM-bl cells (catalog no. 8129) from Dr. John C. Kappes and Dr. Xiaoyun Wu, pCAGGS SF162 gp160 from Drs. L. Stamatatos and C. Cheng-Mayer, anti-HIV immune globulin (HIVIG) from NABI and NHLBI (catalog no. 3957), and anti-HIV-1 p24 monoclonal (183-H12-5C) (catalog no. 3537) from Dr. Bruce Chesebro and Kathy Wehrly. We thank Dr. Kelly Dryden and the University of Virginia Molecular Electron Microscopy Core for training and assistance with cryoET. The University of Virginia Research Computing is acknowledged for high-performance computing time. Cartoons were created with BioRender.com.

Author contributions—A. E. W., O. P., J. M. W., B. K. G.-P., and L. K. T. conceptualization; A. E. W. and B. K. G.-P. data curation; A. E. W. formal analysis; A. E. W. and B. K. G.-P. investigation; A. E. W. and B. K. G.-P. visualization; A. E. W. writing-original draft; V. K. resources; V. K. software; V. K. validation; V. K., O. P., and B. K. G.-P. methodology; O. P., J. M. W., B. K. G.-P., and L. K. T. supervision; J. M. W., B. K. G.-P., and L. K. T. writing-review and editing; L. K. T. funding acquisition.

Funding and additional information—This work was supported by National Institutes of Health Grants R01 AI030557 (to L. K. T.), F30 HD101348 (to A. E. W.), and P50 AI150464 (to B. K. G.-P.). The University of Virginia Molecular Electron Microscopy Core is supported in part by NIH grant U24 GM116790. The content is solely the responsibility of the authors and does not necessarily represent the official views of the National Institutes of Health.

Conflict of interest—The authors declare that they have no conflicts of interest with the contents of this article.

Abbreviations—The abbreviations used are: cryoET, cryo-electron tomography; GPMV, giant plasma membrane vesicle; TIRF, total internal reflection fluorescence; SPPM, supported planar plasma membrane; ROI, region of interest; DMPE, dimyristoylphosphatidylethanolamine; IP6, inositol hexaphosphate.

References

1. Melikyan, G. B. (2011) Membrane fusion mediated by human immunodeficiency virus envelope glycoprotein. *Curr. Top. Membr.* **68,** 81–106 CrossRef Medline
2. Blumenthal, R., Durell, S., and Viard, M. (2012) HIV entry and envelope glycoprotein-mediated fusion. *J. Biol. Chem.* **287,** 40841–40849 CrossRef Medline
3. Chen, B. (2019) Molecular mechanism of HIV-1 entry. *Trends Microbiol.* **27,** 878–891 CrossRef Medline
4. Sougrat, R., Bartesaghi, A., Lifson, J. D., Bennett, A. E., Bess, J. W., Zabransky, D. J., and Subramaniam, S. (2007) Electron tomography of the contact between T cells and SIV/HIV-1: implications for viral entry. *PLoS Pathog.* **3,** e63 CrossRef Medline
5. Gui, L., Ebner, J. L., Mileant, A., Williams, J. A., and Lee, K. K. (2016) Visualization and sequencing of membrane remodeling leading to influenza virus fusion. *J. Virol.* **90,** 6948–6962 CrossRef Medline
6. Lee, K. K. (2010) Architecture of a nascent viral fusion pore. *EMBO J.* **29,** 1299–1311 CrossRef Medline
7. Chlanda, P., Mekhedov, E., Waters, H., Schwartz, C. L., Fischer, E. R., Ryham, R. J., Cohen, F. S., Blank, P. S., and Zimmerberg, J. (2016) The hemifusion structure induced by influenza virus haemagglutinin is determined by physical properties of the target membranes. *Nat. Microbiol.* **1,** 16050 CrossRef Medline
8. Sezgin, E., Kaiser, H.-J., Baumgart, T., Schwille, P., Simons, K., and Levental, I. (2012) Elucidating membrane structure and protein behavior using giant plasma membrane vesicles. *Nat. Protoc.* **7,** 1042–1051 CrossRef Medline
9. Yang, S. T., Kreutzberger, A. J. B., Kiessling, V., Ganser-Pornillos, B. K., White, J. M., and Tamm, L. K. (2017) HIV virions sense plasma membrane heterogeneity for cell entry. *Sci. Adv.* **3,** e1700338 CrossRef Medline
10. Usami, Y., Wu, Y., and Göttlinger, H. G. (2015) SERINC3 and SERINC5 restrict HIV-1 infectivity and are counteracted by Nef. *Nature* **526,** 218–223 CrossRef Medline
11. Rosa, A., Chande, A., Ziglio, S., De Sanctis, V., Bertorelli, R., Goh, S. L., McCauley, S. M., Nowosielska, A., Antonarakis, S. E., Luban, J., Santoni, F. A., and Pizzato, M. (2015) HIV-1 Nef promotes infection by excluding SERINC5 from virion incorporation. *Nature* **526,** 212–217 CrossRef Medline
12. Inuzuka, M., Hayakawa, M., and Ingi, T. (2005) Serinc, an activity-regulated protein family, incorporates serine into membrane lipid synthesis. *J. Biol. Chem.* **280,** 35776–35783 CrossRef Medline
13. Zhang, X., Zhou, T., Yang, J., Lin, Y., Shi, J., Zhang, X., Frabutt, D. A., Zeng, X., Li, S., Venta, P. J., and Zheng, Y.-H. (2017) Identification of SERINC5-001 as the predominant spliced isoform for HIV-1 restriction. *J. Virol.* **91,** e00137-17 CrossRef Medline
14. Chen, Y.-C., Sood, C., Marin, M., Aaron, J., Gratton, E., Salaita, K., and Melikyan, G. B. (2020) Super-resolution fluorescence imaging reveals that serine incorporator protein 5 inhibits human immunodeficiency virus fusion by disrupting envelope glycoprotein clusters. *ACS Nano* CrossRef CrossRef Medline
15. Schulte, B., Selyutina, A., Opp, S., Herschhorn, A., Sodroski, J. G., Pizzato, M., and Diaz-Griffero, F. (2018) Localization to detergent-resistant membranes and HIV-1 core entry inhibition correlate with HIV-1 restriction by SERINC5. *Virology* **515,** 52–65 CrossRef Medline
16. Beitari, S., Ding, S., Pan, Q., Finzi, A., and Liang, C. (2017) Effect of HIV-1 Env on SERINC5 antagonism. *J. Virol.* **91,** e02214-16 CrossRef Medline
17. Sood, C., Marin, M., Chande, A., Pizzato, M., and Melikyan, G. B. (2017) SERINC5 protein inhibits HIV-1 fusion pore formation by promoting functional inactivation of envelope glycoproteins. *J. Biol. Chem.* **292,** 6014–6026 CrossRef Medline
18. Pye, V. E., Rosa, A., Bertelli, C., Struwe, W. B., Maslen, S. L., Corey, R., Liko, I., Hassall, M., Mattiuzzo, G., Ballandras-Colas, A., Nans, A., Takeuchi, Y., Stansfeld, P. J., Skehel, J. M., Robinson, C. V., *et al.* (2020) A bipartite structural organization defines the SERINC family of HIV-1 restriction factors. *Nat. Struct. Mol. Biol.* **27,** 78–83 CrossRef Medline
19. Trautz, B., Wiedemann, H., Lüchtenborg, C., Pierini, V., Kranich, J., Glass, B., Kräusslich, H.-G., Brocker, T., Pizzato, M., Ruggieri, A., Brügger, B., and Fackler, O. T. (2017) The host-cell restriction factor SERINC5 restricts HIV-1 infectivity without altering the lipid composition and organization of viral particles. *J. Biol. Chem.* **292,** 13702–13713 CrossRef Medline
20. Firrito, C., Bertelli, C., Vanzo, T., Chande, A., and Pizzato, M. (2018) SERINC5 as a new restriction factor for human immunodeficiency virus

and murine leukemia virus. *Annu. Rev. Virol.* **5,** 323–340 CrossRef Medline
21. Sood, C., Marin, M., Mason, C. S., and Melikyan, G. B. (2016) Visualization of content release from cell surface-attached single HIV-1 particles carrying an extra-viral fluorescent pH-sensor. *PLoS ONE* **11,** e0148944 CrossRef Medline
22. Floyd, D. L., Ragains, J. R., Skehel, J. J., Harrison, S. C., and van Oijen, A. M. (2008) Single-particle kinetics of influenza virus membrane fusion. *Proc. Natl. Acad. Sci. U.S.A.* **105,** 15382–15387 CrossRef Medline
23. Kreutzberger, A. J. B., Kiessling, V., Liang, B., Seelheim, P., Jakhanwal, S., Jahn, R., Castle, J. D., and Tamm, L. K. (2017) Reconstitution of calcium-mediated exocytosis of dense-core vesicles. *Sci. Adv.* **3,** e1603208 CrossRef Medline
24. Liu, S., Lu, H., Niu, J., Xu, Y., Wu, S., and Jiang, S. (2005) Different from the HIV fusion inhibitor C34, the anti-HIV drug Fuzeon (T-20) inhibits HIV-1 entry by targeting multiple sites in gp41 and gp120. *J. Biol. Chem.* **280,** 11259–11273 CrossRef Medline
25. Maurer, U. E., Sodeik, B., and Grünewald, K. (2008) Native 3D intermediates of membrane fusion in herpes simplex virus 1 entry. *Proc. Natl. Acad. Sci. U. S. A.* **105,** 10559–10564 CrossRef Medline
26. Stano, A., Leaman, D. P., Kim, A. S., Zhang, L., Autin, L., Ingale, J., Gift, S. K., Truong, J., Wyatt, R. T., Olson, A. J., and Zwick, M. B. (2017) Dense array of spikes on HIV-1 virion particles. *J. Virol.* **91,** e00415-17 CrossRef Medline
27. Dai, W., Usami, Y., Wu, Y., and Göttlinger, H. (2018) A long cytoplasmic loop governs the sensitivity of the anti-viral host protein SERINC5 to HIV-1 Nef. *Cell Rep.* **22,** 869–875 CrossRef Medline
28. Sharma, S., Lewinski, M. K., and Guatelli, J. (2018) An *N*-glycosylated form of SERINC5 is specifically incorporated into HIV-1 virions. *J. Virol.* **92,** e00753-18 CrossRef Medline
29. Shi, J., Xiong, R., Zhou, T., Su, P., Zhang, X., Qiu, X., Li, H., Li, S., Yu, C., Wang, B., Ding, C., Smithgall, T. E., and Zheng, Y.-H. (2018) HIV-1 Nef antagonizes SERINC5 restriction by downregulation of SERINC5 via the endosome/lysosome system. *J. Virol.* **92,** e00196-18 CrossRef Medline
30. Passos, V., Zillinger, T., Casartelli, N., Wachs, A. S., Xu, S., Malassa, A., Steppich, K., Schilling, H., Franz, S., Todt, D., Steinmann, E., Sutter, K., Dittmer, U., Bohne, J., Schwartz, O., *et al.* (2019) Characterization of endogenous SERINC5 protein as anti-HIV-1 factor. *J. Virol.* **93,** e01221-19 CrossRef Medline
31. Rawle, R. J., Villamil Giraldo, A. M., Boxer, S. G., and Kasson, P. M. (2019) Detecting and controlling dye effects in single-virus fusion experiments. *Biophys. J.* **117,** 445–452 CrossRef Medline
32. Hughes, L. D., Rawle, R. J., and Boxer, S. G. (2014) Choose your label wisely: water-soluble fluorophores often interact with lipid bilayers. *PLoS ONE* **9,** e87649 CrossRef Medline
33. Blumenthal, R., Gallo, S. A., Viard, M., Raviv, Y., and Puri, A. (2002) Fluorescent lipid probes in the study of viral membrane fusion. *Chem. Phys. Lipids* **116,** 39–55 CrossRef Medline
34. Dufourc, E. J., Smith, I. C. P., and Jarrell, H. C. (1984) Interaction of amphotericin B with membrane lipids as viewed by 2H-NMR. *Biochim. Biophys. Acta* **778,** 435–442 CrossRef Medline
35. Cohen, F. S., and Melikyan, G. B. (2004) The energetics of membrane fusion from binding, through hemifusion, pore formation, and pore enlargement. *J. Membr. Biol.* **199,** 1–14 CrossRef Medline
36. Kawamoto, S., and Shinoda, W. (2014) Free energy analysis along the stalk mechanism of membrane fusion. *Soft Matter* **10,** 3048–3054 CrossRef Medline
37. Sergi, P.-P., Marin, M., Gahlaut, N., Suter, R., Kondo, N., and Melikyan, G. B. (2013) Fusion of mature HIV-1 particles leads to complete release of a Gag-GFP-based content marker and raises the intraviral pH. *PLoS ONE* **8,** e71002 CrossRef Medline
38. Cheng-Mayer, C., Liu, R., Landau, N. R., and Stamatatos, L. (1997) Macrophage tropism of human immunodeficiency virus type 1 and utilization of the CC-CKR5 coreceptor. *J. Virol.* **71,** 1657–1661 CrossRef Medline
39. Stamatatos, L., Lim, M., and Cheng-Mayer, C. (2000) Generation and structural analysis of soluble oligomeric gp140 envelope proteins derived from neutralization-resistant and neutralization-susceptible primary HIV type 1 isolates. *AIDS Res. Hum. Retroviruses* **16,** 981–994 CrossRef Medline
40. Stamatatos, L., Wiskerchen, M., and Cheng-Mayer, C. (1998) Effect of major deletions in the V1 and V2 loops of a macrophage-tropic HIV type 1 isolate on viral envelope structure, cell entry, and replication. *AIDS Res. Hum. Retroviruses* **14,** 1129–1139 CrossRef Medline
41. Hulseberg, C. E., Fénéant, L., Wijs, K. M. S., Kessler, N. P., Nelson, E. A., Shoemaker, C. J., Schmaljohn, C. S., Polyak, S. J., and White, J. M. (2019) Arbidol and other low-molecular-weight drugs that inhibit Lassa and Ebola viruses. *J. Virol.* **93,** e02185-18 CrossRef Medline
42. Wehrly, K., and Chesebro, B. (1997) p24 antigen capture assay for quantification of human immunodeficiency virus using readily available inexpensive reagents. *Methods* **12,** 288–293 CrossRef Medline
43. Toohey, K., Wehrly, K., Nishio, J., Perryman, S., and Chesebro, B. (1995) Human immunodeficiency virus envelope V1 and V2 regions influence replication efficiency in macrophages by affecting virus spread. *Virology* **213,** 70–79 CrossRef Medline
44. Cummins, L. M., Weinhold, K. J., Matthews, T. J., Langlois, A. J., Perno, C. F., Condie, R. M., and Allain, J. P. (1991) Preparation and characterization of an intravenous solution of IgG from human immunodeficiency virus-seropositive donors. *Blood* **77,** 1111–1117 CrossRef Medline
45. Derdeyn, C. A., Decker, J. M., Sfakianos, J. N., Wu, X., O'Brien, W. A., Ratner, L., Kappes, J. C., Shaw, G. M., and Hunter, E. (2000) Sensitivity of human immunodeficiency virus type 1 to the fusion inhibitor T-20 is modulated by coreceptor specificity defined by the V3 loop of gp120. *J. Virol.* **74,** 8358–8367 CrossRef Medline
46. Platt, E. J., Bilska, M., Kozak, S. L., Kabat, D., and Montefiori, D. C. (2009) Evidence that ecotropic murine leukemia virus contamination in TZM-bl cells does not affect the outcome of neutralizing antibody assays with human immunodeficiency virus type 1. *J. Virol.* **83,** 8289–8292 CrossRef Medline
47. Takeuchi, Y., McClure, M. O., and Pizzato, M. (2008) Identification of gammaretroviruses constitutively released from cell lines used for human immunodeficiency virus research. *J. Virol.* **82,** 12585–12588 CrossRef Medline
48. Wei, X., Decker, J. M., Liu, H., Zhang, Z., Arani, R. B., Kilby, J. M., Saag, M. S., Wu, X., Shaw, G. M., and Kappes, J. C. (2002) Emergence of resistant human immunodeficiency virus type 1 in patients receiving fusion inhibitor (T-20) monotherapy. *Antimicrob. Agents Chemother.* **46,** 1896–1905 CrossRef Medline
49. Sarzotti-Kelsoe, M., Bailer, R. T., Turk, E., Lin, C., Bilska, M., Greene, K. M., Gao, H., Todd, C. A., Ozaki, D. A., Seaman, M. S., Mascola, J. R., and Montefiori, D. C. (2014) Optimization and validation of the TZM-bl assay for standardized assessments of neutralizing antibodies against HIV-1. *J. Immunol. Methods* **409,** 131–146 CrossRef Medline
50. Kalb, E., Frey, S., and Tamm, L. K. (1992) Formation of supported planar bilayers by fusion of vesicles to supported phospholipid monolayers. *Biochim. Biophys. Acta* **1103,** 307–316 CrossRef Medline
51. Wagner, M. L., and Tamm, L. K. (2000) Tethered polymer-supported planar lipid bilayers for reconstitution of integral membrane proteins: silane-polyethyleneglycol-lipid as a cushion and covalent linker. *Biophys. J.* **79,** 1400–1414 CrossRef Medline
52. Dick, R. A., Zadrozny, K. K., Xu, C., Schur, F. K. M., Lyddon, T. D., Ricana, C. L., Wagner, J. M., Perilla, J. R., Ganser-Pornillos, B. K., Johnson, M. C., Pornillos, O., and Vogt, V. M. (2018) Inositol phosphates are assembly co-factors for HIV-1. *Nature* **560,** 509–512 CrossRef Medline

53. Skinkle, A. (2019) Cell-derived plasma membrane vesicles are permeable to hydrophilic macromolecules. *Biophys. J.* **118,** 1292–1300 CrossRef Medline
54. Zheng, S. Q., Palovcak, E., Armache, J.-P., Verba, K. A., Cheng, Y., and Agard, D. A. (2017) MotionCor2: anisotropic correction of beam-induced motion for improved cryo-electron microscopy. *Nat. Methods* **14,** 331–332 CrossRef Medline
55. Mastronarde, D. N., and Held, S. R. (2017) Automated tilt series alignment and tomographic reconstruction in IMOD. *J. Struct. Biol* **197,** 102–113 CrossRef Medline
56. Buchholz, T.-O., Jordan, M., Pigino, G., and Jug, F. (2018) Cryo-CARE: content-aware image restoration for cryo-transmission electron microscopy data. *arXiv* 502–506 CrossRef